Role of the kinematics of probing electrons in electron energy-loss spectroscopy of solid surfaces

V. U. Nazarov*
Research Center for Applied Sciences, Academia Sinica, Taipei 11529, Taiwan

V. M. Silkin and E. E. Krasovskii
Departamento de Física de Materiales, Facultad de Ciencias Quíimicas, Universidad del Pais Vasco/Euskal Herriko Unibertsitatea, Apartado Postal 1072, San Sebastián/Donostia, 20080 Basque Country, Spain;
Donostia International Physics Center, Paseo Manuel de Lardizabal 4, San Sebastián/Donostia, 20018 Basque Country, Spain;
and IKERBASQUE, Basque Foundation for Science, 48013 Bilbao, Spain
(Received 8 November 2015; published 4 January 2016)

Inelastic scattering of electrons incident on a solid surface is determined by two properties: (i) electronic response of the target system and (ii) the detailed quantum-mechanical motion of the projectile electron inside and in the vicinity of the target. We emphasize the equal importance of the second ingredient, pointing out the fundamental limitations of the conventionally used theoretical description of the electron energy-loss spectroscopy (EELS) in terms of the "energy-loss functions." Our approach encompasses the dipole and impact scattering as specific cases, with the emphasis on the quantum-mechanical treatment of the probe electron. Applied to the high-resolution EELS of Ag surface, our theory largely agrees with recent experiments, while some instructive exceptions are rationalized.

DOI: 10.1103/PhysRevB.93.035403

I. INTRODUCTION

Electron energy-loss spectroscopy (EELS) is an efficient and widely used experimental method to study excitation processes on clean and adsorbate-covered surfaces of solids and in thin (including atomically thin) films [1–4]. This method utilizes the inelastic scattering of electrons, resulting in both energy and momentum transfer from the projectiles to diverse kinds of excitations in the samples. Reflected or transmitted electrons are analyzed with respect to the energy and momentum loss they have experienced in the interaction with a target, revealing a wealth of information about the properties of the latter.

Much effort has been exerted over the years to complement EELS experimental techniques with comprehensive theoretical pictures [2,5–11]. In this way, a clear understanding of elementary excitations [such as electron-hole pair generation, collective electronic excitations (plasmons), atomic vibrational modes, etc.], including their momentum dispersion, for solid surfaces, for interfaces, and in thin films has been achieved.

Presently, the main approach to interpret EELS data theoretically is to use *energy-loss functions*. A clear example is the surface energy-loss function of a semi-infinite solid, which, neglecting the momentum dispersion, can be written as [10]

$$L_s(\omega) = -\mathrm{Im}\frac{1}{\varepsilon(\omega)+1}, \tag{1}$$

where $\varepsilon(\omega)$ is the frequency-dependent dielectric function (DF) of the bulk solid. This example exhibits an important feature common also to other much more sophisticated loss functions: $L_s(\omega)$ of Eq. (1) is a property of only the target. Indeed, it is not concerned with the setup of the EELS experiment, such as the angles of incidence and reflection (or transmission); the energy of the electrons in the incident beam; or, which is subtler, the detailed, preferably quantum-mechanical motion of the probe electrons both outside and inside the target. As a clear reason why such an approach may not be adequate, we note that it cannot, in principle, determine the relative intensities of the surface and the bulk plasmons in a given EELS setup, with the bulk response being given in the same approximation by another energy-loss function $L_b(\omega) = -\mathrm{Im}\frac{1}{\varepsilon(\omega)}$. For systems where the bulk and the surface excitations overlap, as is the case, e.g., for silver, this constitutes a serious limitation.

Meanwhile, a theoretical approach to EELS taking full account of the incident electron kinematics was introduced two decades ago [12]. This is based on the solution to the problem of the energy loss by an electron traveling in the lattice potential of a target, utilizing the method known in the scattering theory as the *distorted-wave approximation* [13] [see Eq. (2) in the next section]. That formal theory of the response of the target system coupled to the quantum-mechanical motion of the projectile electron has, however, never been implemented to the full extent in calculations for specific systems. Indeed, the formalism importantly stipulates that the density-functional theory [14] (DFT) potential used in the calculations of the ground state and of the response of the target, on the one hand, and the potential which determines the motion of the projectile electron, on the other, should be the same crystalline potential. Only two specific applications of the theory have been made so far. In the first, the theory of Ref. [12] has been implemented for jellium within a model of the incident electron reflected from an infinite barrier at a given position above/below the surface [15]. In the other, which is an application to the inelastic low-energy electron diffraction (LEED) of simple metals, a severe approximation of the kinematic diffraction theory was used [16]. At the same time, detailed measurements in the high-resolution EELS (HREELS) of the silver surface in the wide energy range have become available recently [17],

*nazarov@gate.sinica.edu.tw

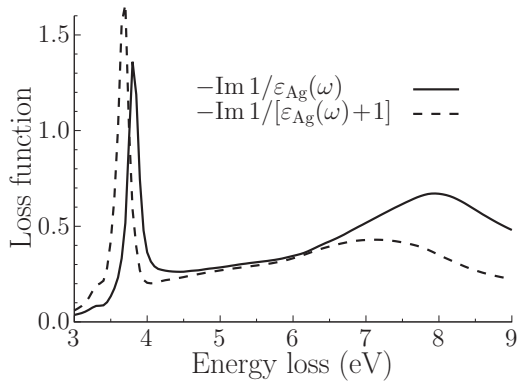

FIG. 1. Bulk (solid line) and surface (dashed line) energy-loss functions of silver. The experimental optical dielectric function $\varepsilon_{\mathrm{Ag}}(\omega)$ is used [18].

calling for the implementation of refined theoretical methods.

The purpose of this paper is therefore twofold. First, we aim at the implementation of the theory of EELS of Ref. [12] in its original form, i.e., that would treat the incident electron and the electrons of the target system on the same footing. Second, we apply this theory to the EELS of the Ag surface, which is exactly the case when the interplay of the response of the target with the details of the probe's motion is especially important due to the overlap of the bulk and the surface features in the excitation spectrum of this material, as illustrated in Fig. 1. By this we both further advance the theory of EELS and achieve an improvement in the understanding of the experimental spectra of the Ag surface.

Since the fully *ab initio* solution to the problem of the dielectric response of *d* metals still remains a computationally formidable task, we have to resort to some model considerations. First, we substitute the three-dimensional (3D) problem with a one-dimensional (1D) one, neglecting the system's nonuniformity in the surface plane. Second, the *d* electrons are included in a phenomenological way, using the model of Liebsch [9,19] for the background DF. This work should therefore be considered a step forward toward the full-feature 3D implementation of the same method, also treating *d* electrons *ab initio*. However, the main ingredients of the theory (among them, importantly, the necessary inclusion of the optical potential) are presented and discussed in this work, facilitating the future implementation of the method in full.

This paper is organized as follows. In Sec. II we review and further work out details of including the motion of the scattered electrons in the theory of EELS. In Sec. III, results of the calculations conducted with the use of our theory are presented and discussed. Conclusions are collected in Sec. IV. In the Appendix we detail some important properties of the model utilized in the calculations. We use atomic units ($e^2 = \hbar = m_e = 1$) throughout unless otherwise indicated.

II. FORMALISM

A formal solution to the problem of the inelastic scattering of an electron in the EELS setup, which incorporates the detailed quantum-mechanical motion of the projectile, can be quite generally written as [12,16]

$$\frac{d^2\sigma}{d\omega d\Omega}(\mathbf{p}' \leftarrow \mathbf{p}) = -\frac{16\pi^3 p'}{p}\mathrm{Im}\int \frac{\rho^*_{\mathrm{ext}}(\mathbf{r}'')}{|\mathbf{r}''-\mathbf{r}|}\chi(\mathbf{r},\mathbf{r}',\omega) \times \frac{\rho_{\mathrm{ext}}(\mathbf{r}''')}{|\mathbf{r}'-\mathbf{r}'''|}d\mathbf{r}d\mathbf{r}'d\mathbf{r}''d\mathbf{r}''', \tag{2}$$

where the left-hand side of Eq. (2) is the differential cross section of the scattering from the state of the momentum $\mathbf{p}$ to a state of the momentum within the solid angle $d\Omega$ around $\mathbf{p}'$, with an energy loss within $d\omega$ around $\omega = (p^2 - p'^2)/2$. On the right-hand side of Eq. (2), $\chi(\mathbf{r},\mathbf{r}',\omega)$ is the interacting-electron [20] density-response function of the target, and the complex-valued "external charge density"

$$\rho_{\mathrm{ext}}(\mathbf{r}) = \langle \mathbf{r}|\mathbf{p}^+\rangle^* \langle \mathbf{r}|\mathbf{p}'^-\rangle \tag{3}$$

is determined by the *elastic* scattering *incoming* and *outgoing* wave functions, $|\mathbf{p}^+\rangle$ and $|\mathbf{p}^-\rangle$, respectively, which are the solutions to the Lippmann-Schwinger equation [13]

$$\langle \mathbf{r}|\mathbf{p}^\pm\rangle = \langle \mathbf{r}|\mathbf{p}\rangle + G^0\left(\frac{p^2}{2} \pm \mathrm{i}0_+\right)V_l(\mathbf{r})\langle \mathbf{r}|\mathbf{p}^\pm\rangle, \tag{4}$$

where $G^0(E)$ is the noninteracting Green's function, $V_l(\mathbf{r})$ is the single-particle static lattice potential, and $\langle \mathbf{r}|\mathbf{p}\rangle = e^{\mathrm{i}\mathbf{p}\cdot\mathbf{r}}/(2\pi)^{3/2}$ are plane waves. [21]

The structure of Eq. (2) has a transparent physical interpretation: The external charge ρ_{ext} creates an external Coulomb potential, which, through the density-response function χ, induces the charge fluctuation in the target. Finally, the Coulomb potential of that fluctuation couples to the external charge itself, causing the inelastic scattering of the latter.

It must be, however, emphasized that the above picture is no more than a convenient verbal description of the strict mathematical formalism presented in Ref. [12]: The derivation of Eq. (2) does not rely on the substitution of the true quantum-mechanical scattering problem for an electron with an artificial charge density. It rather solves the problem of the combined elastic and inelastic scattering of a charge in an arbitrary many- (or few-) body system, which, with the mild assumption that the impinging electron can be considered distinguishable from those of the target, can be put into the terms of the density-response function of the target and the elastic scattering states of the projectile. Obtained within the distorted-wave approximation [13], Eq. (2) is exact to first order in the inelastic processes (the first Born approximation), and it is exact to *all* orders in the elastic scattering. It includes both the long- and the short-range interactions of the probe electron with the target, i.e., the dipole and impact scattering [10], respectively, within, most importantly, the quantum-mechanical treatment of the probe itself.

Of course, practically, the quality of specific calculations by Eq. (2) depends on the accuracy of the approximations used to calculate its ingredients, i.e., the density-response function of the target χ and the wave functions of the incoming and outgoing electrons utilized in the construction of ρ_{ext}. We now turn to the use of specific models.

A. Model of a laterally uniform target

In this work we will use a simplification of the potential $V_l(\mathbf{r}) = V_l(z)$ averaged in the plane parallel to the surface, which is chosen as the xy plane, with the z axis normal to the surface and directed into vacuum. In this case the wave functions are plane waves in the direction parallel to the surface,

$$\langle \mathbf{r}|\mathbf{p}^{\pm}\rangle = \langle z|p_z^{\pm}\rangle \frac{e^{i\mathbf{p}_\parallel\cdot\mathbf{r}_\parallel}}{2\pi}, \tag{5}$$

where the subscript parallel symbol denotes the xy projection of a vector. To take advantage of the scattering theory framework, in the following we represent the target with a sufficiently thick slab, with vacuum both above and below, which is also consistent with our numerical implementation of the method. Then $\langle z|p_z^{+}\rangle$ can be conveniently found as a solution to the Schrödinger equation with the following asymptotic boundary conditions:

$$\langle z|p_z^{+}\rangle = \frac{1}{2\pi}\begin{cases} a^+e^{ip_z z} + b^+e^{-ip_z z}, & z\to+\infty, \\ c^+e^{ip_z z} + d^+e^{-ip_z z}, & z\to-\infty, \end{cases} \tag{6}$$

$$\begin{aligned} p_z > 0 &: c^+ = 1, \quad b^+ = 0, \\ p_z < 0 &: a^+ = 1, \quad d^+ = 0. \end{aligned} \tag{7}$$

The asymptotic of $\langle z|p_z'^{-}\rangle$ is easily obtained from the relation

$$\langle z|p_z'^{-}\rangle = \langle z| - p_z'^{+}\rangle^*. \tag{8}$$

Therefore, using Eqs. (6) and (7), we have

$$\langle z|p_z'^{-}\rangle = \frac{1}{2\pi}\begin{cases} a^-e^{ip_z' z} + b^-e^{-ip_z' z}, & z\to+\infty, \\ c^-e^{ip_z' z} + d^-e^{-ip_z' z}, & z\to-\infty, \end{cases} \tag{9}$$

$$\begin{aligned} p_z' > 0 &: a^- = 1, \quad d^- = 0, \\ p_z' < 0 &: c^- = 1, \quad b^- = 0. \end{aligned} \tag{10}$$

Equation (6) together with the bottom line of Eq. (7) describes the electron incident on the surface, as in the low-energy electron diffraction (LEED) experiment. Interestingly, the wave function of Eq. (9) together with the top line of Eq. (10) is a time-reversed LEED state. This kind of function describes the photoelectron (PE) final state in the one-step theory of photoemission [22]. Note that in vacuum it contains both outgoing and incoming beams. Thus, while in the LEED and PE setups each of these kinds of the wave functions enters separately, in EELS they are present together.

For $\rho_{\rm ext}(\mathbf{r})$ we can write

$$\rho_{\rm ext}(\mathbf{r}) = \rho_{\rm ext}(z)\frac{e^{i\mathbf{q}_\parallel\cdot\mathbf{r}_\parallel}}{(2\pi)^2}, \tag{11}$$

where

$$\rho_{\rm ext}(z) = \langle z|p_z^{+}\rangle^*\langle z|p_z'^{-}\rangle, \tag{12}$$

and $\mathbf{q}_\parallel = \mathbf{p}_\parallel - \mathbf{p}_\parallel'$. Then, finally, Eq. (2) takes the convenient form

$$\begin{aligned} \frac{1}{A}\frac{d^2\sigma}{d\omega d\Omega}(\mathbf{p}'\leftarrow\mathbf{p}) = -\frac{p'}{\pi p\, q_\parallel^2}\,\mathrm{Im}\int \rho_{\rm ext}^*(z'')e^{-q_\parallel|z''-z|} \\ \times\chi(z,z',q_\parallel,\omega)e^{-q_\parallel|z'-z'''|}\rho_{\rm ext}(z''') \\ \times dz\,dz'\,dz''\,dz''', \end{aligned} \tag{13}$$

where A is the surface normalization area.

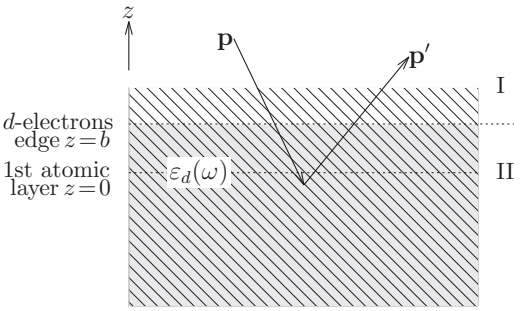

FIG. 2. Schematics of the model used in the calculation.

B. Real-space solution with the background dielectric function

According to Eq. (13), the external potential applied to our system is

$$\phi_{\rm ext}(z) = \frac{2\pi}{q_\parallel}\int e^{-q_\parallel|z-z'|}\rho_{\rm ext}(z')dz'. \tag{14}$$

Therefore, Eq. (13) can be rewritten as

$$\frac{1}{A}\frac{d\sigma}{d\omega d\Omega}(\mathbf{p}'\leftarrow\mathbf{p}) = -\frac{p'}{4\pi^3 p}\,\mathrm{Im}\int \rho_{\rm ext}^*(z'')\phi_{\rm ind}(z)dz, \tag{15}$$

where

$$\phi_{\rm ind}(z) = \frac{2\pi}{q_\parallel}\int e^{-q_\parallel|z'-z|}\chi(z',z'',q_\parallel,\omega)\phi_{\rm ext}(z'')dz'dz'' \tag{16}$$

is the potential induced in the system in response to the external charge density $\rho_{\rm ext}(z)$. To determine $\phi_{\rm ind}(z)$, a simplified model of the Ag surface, introduced by Liebsch [9,19], is used, in which only s electrons are treated quantum mechanically through the calculation of their response function, while the influence of d electrons is included effectively by the use of a background DF $\epsilon_d(\omega)$ comprising the half-space $z \leqslant b$, as schematized in Fig. 2. Then, for the total scalar potential $\phi(z) = \phi_{\rm ext}(z) + \phi_{\rm ind}(z)$ we can write separately in regions I (with $z \geqslant b$) and II (with $z \leqslant b$)

$$\phi(z) = \begin{cases} \tilde\phi(z) + Ae^{-q_\parallel z}, & z \geqslant b, \\ \frac{\tilde\phi(z)}{\epsilon_d} + Be^{q_\parallel z}, & z \leqslant b, \end{cases} \tag{17}$$

where

$$\tilde\phi(z) = \phi_{\rm ext}(z) + \phi_s(z), \tag{18}$$

$\phi_s(z)$ is the potential of the response of only s electrons, and A and B are constants to be determined from the boundary conditions of the continuity of the tangential component of the electric field and the normal component of the electric displacement vector, which give, respectively,

$$\begin{aligned} \tilde\phi(b) + Ae^{-q_\parallel b} &= \frac{\tilde\phi(b)}{\epsilon_d} + Be^{q_\parallel b}, \\ -Ae^{-q_\parallel b} &= Be^{q_\parallel b}\epsilon_d. \end{aligned} \tag{19}$$

For ϕ_s we can write

$$\begin{aligned} \phi_s(z) = \frac{2\pi}{q_\parallel}\int e^{-q_\parallel|z-z'|}\chi_s(z',z'',q_\parallel,\omega) \\ \times[\phi(z'') - \phi_s(z'')]dz'dz'', \end{aligned} \tag{20}$$

where χ_s is the density-response function of only s electrons. By further rewriting Eq. (17) as

$$\phi(z) - \phi_s(z) = \begin{cases} \phi_{\rm ext}(z) + Ae^{-q_\parallel z}, & z \geqslant b, \\ \frac{\phi_{\rm ext}(z)}{\epsilon_d} + \left(\frac{1}{\epsilon_d} - 1\right)\phi_s(z) + Be^{q_\parallel z}, & z \leqslant b, \end{cases} \quad (21)$$

and substituting Eq. (21) into the right-hand side of Eq. (20) and Eq. (18) into Eqs. (19), we arrive at a closed system of equations for $\phi_s(z)$, A, and B, which is numerically solved on a grid of z. Then from $\phi_s(z)$ we obtain $\tilde{\phi}(z)$ from Eq. (18), $\phi(z)$ from Eq. (17), and $\phi_{\rm ind}(z)$ as $\phi(z) - \phi_{\rm ext}(z)$. The latter is finally used in Eq. (15) to calculate the EEL spectrum.

III. CALCULATIONS, RESULTS, AND DISCUSSION

Our calculation of the ground state of the s electrons of Ag(111) uses the 1D interpolation of the surface and the bulk potential of Ref. [23]. A supercell with period $d = 221.7$ a.u. was used, which included 31 layers of the model s subsystem of Ag; the rest were occupied with vacuum. The time-dependent density-functional theory (TDDFT) calculation of the density-response function $\chi_s(z,z',q_\parallel,\omega)$ is performed on the level of the random-phase approximation (RPA), i.e., setting the exchange-correlation kernel [24] f_{xc} to zero. Then we apply the procedures from Secs. II B and II A to account for the response of d electrons and to finally obtain the EEL spectra. The edge of the d electrons was set at $b = 0.717$ a.u. above the upper atomic layer. For $\varepsilon_d(\omega)$ we take

$$\varepsilon_d(\omega) = \varepsilon_{\rm Ag}(\omega) - [\varepsilon_s(\omega) - 1] = \varepsilon_{\rm Ag}(\omega) + \frac{\omega_p^2}{\omega^2}, \quad (22)$$

where $\varepsilon_{\rm Ag}(\omega)$ is the experimental optical DF of silver [18] and $\varepsilon_s(\omega) = 1 - \omega_p^2/\omega^2$ is the Drude DF of s electrons with the plasma frequency $\omega_p = 9$ eV.

To construct $\rho_{\rm ext}(z)$ by Eq. (12), we solved the Schrödinger equation with the asymptotic boundary conditions of Eqs. (6) and (9). The scattering wave functions were obtained by solving the inverse band-structure problem as explained in Ref. [25] and matching the Bloch solutions in the crystal to the linear combination of the incident and reflected waves in the vacuum. The same crystal potential as for the evaluation of χ was used, with the addition of the absorbing imaginary potential $-iV_{\rm i}$, as explained below. Importantly, similar to the LEED theory [26], the inclusion of the optical potential (OP) in the Hamiltonian is necessary for EELS theory as well. This can be understood considering that, without OP, electrons that have taken an arbitrarily long round-trip into the depth of the sample would contribute to the spectrum. Since, in the first Born approximation, the probability of the bulk energy loss is proportional to the path length traveled, this would make the intensity of the bulk losses infinitely high. The influence of the deep interior of the sample is, however, suppressed in LEED by all the inelastic processes and in EELS by the inelastic processes beyond the first Born approximation. In the present calculation $V_{\rm i}$ was taken to be spatially constant in the solid and zero in vacuum. At $E_p = 40$ eV, we used $V_{\rm i} = 0.3$ eV for an angle with the normal to the surface of 80°, 75°, 70°, $V_{\rm i} = 0.5$ eV for 85°, and $V_{\rm i} = 0.1$ eV for 55°. In Fig. 3 $\rho_{\rm ext}(z)$ and the corresponding $\phi_{\rm ext}(z)$ are shown for representative values of the parameters of the EELS experiment.

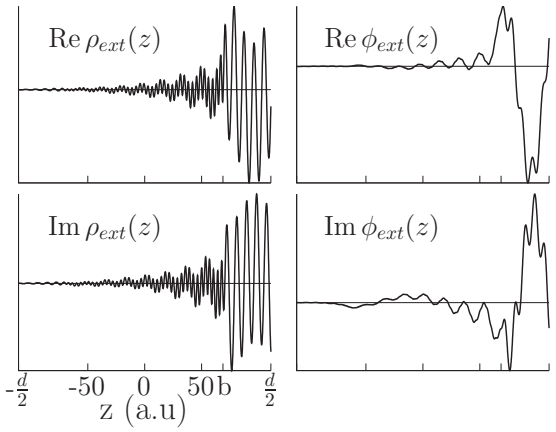

FIG. 3. The complex-valued density of Eq. (12) (left) and the corresponding potential (right) as a function of the coordinate z at $\omega = 3.7$ eV, $\theta_i = 80°$, $\theta_s = 75°$, and $E_p = 40$ eV. At these parameters, $q_\parallel = 0.111$ a.u. The edge of the d electrons is at $b = 67.2$ a.u., and the period of the supercell used in the calculation of the response of s electrons is $d = 221.7$ a.u. In the calculation, the origin is chosen in the center of the supercell.

In Figs. 4 and 5 results of calculations of the EEL reflection spectra are presented. They are compared to experimental HREELS of the system of ten monolayers of Ag on the (111) surface of the Ni substrate [17]. In Fig. 4 the theoretical and experimental EEL spectra are shown for a primary energy of electrons $E_p = 40$ eV, an angle of incidence $\theta_i = 80°$, and three values of the angle of scattering θ_s, 85°, 75°, and 70°. In Fig. 5 the results for the specular geometry with $\theta_i = \theta_s = 55°$ and the same primary energy are presented. The comparison of the theory with the experiment is reasonably good. Most importantly, the sharp bulk and surface plasmon peaks near 3.7 eV, which are separately present in the plots of the corresponding energy-loss functions (Fig. 1), are never resolved from each other in our calculations, but they form a joint broadened peak with a contribution from both types

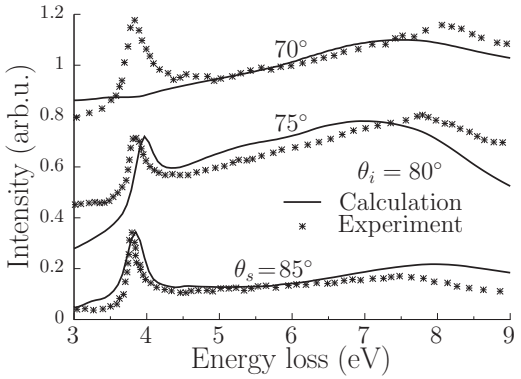

FIG. 4. HREEL spectra of the Ag(111) surface calculated within the framework of our theoretical approach (solid lines) compared to the experimental spectra of ten monolayers of Ag on the Ni(111) surface, the latter compiled from Ref. [17] (symbols). The energy of electrons in the incident beam is $E_p = 40$ eV.

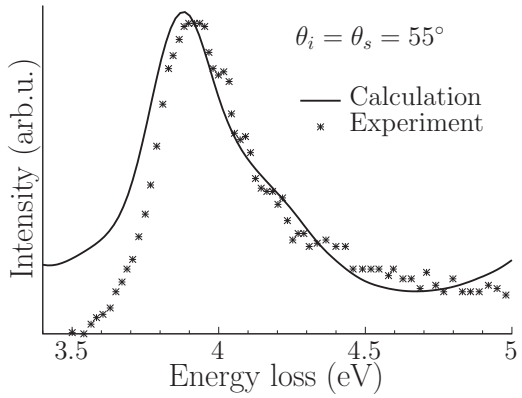

FIG. 5. The same as Fig. 4, but for the specular reflection $\theta_i = \theta_s = 55°$.

of excitations. This is in full agreement with the HREELS experiments [17,27–29]. A notable exception from the agreement between the theory and the experiment is the case of $\theta_i = 80°$ and $\theta_s = 70°$, the top spectrum in Fig. 4, where, surprisingly, the lower-energy plasmon peak, which is strong in the experimental spectrum, is absent in the theoretical one.

To examine the latter discrepancy more closely, in Fig. 6 we plot theoretical spectra for the angle of scattering gradually changing from 75°, when the peak in question is pronounced, to 70°, when this peak disappears. These results show that the strength of the peak near 3.7 eV decreases systematically when the scattering angle $\theta_i - \theta_s$ increases. We note that a similar effect of the disappearance of the 3.7 eV peak with the growing momentum can be observed in the results of the calculations of Ref. [30], performed in the dipole-scattering mode within the same model of d electrons. We analyze this tendency in detail in Appendix with the conclusion that, although the background DF model is applicable in the higher energy range around 8 eV to account for the bulk, surface, and multipole plasmons in Ag [9,19], it fails for the lower-energy plasmons at larger values of the wave vector. Obviously, the future theory, which will include d electrons from first principles, will be free from this deficiency.

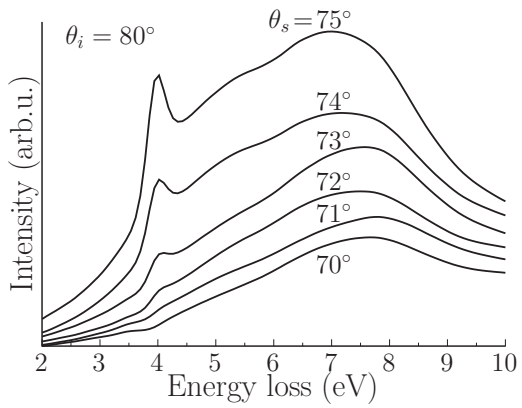

FIG. 6. The calculated EEL spectra for the angle of scattering changing from 75° to 70° with a step of 1°. The gradual disappearance of the peak around 3.7 eV can be observed.

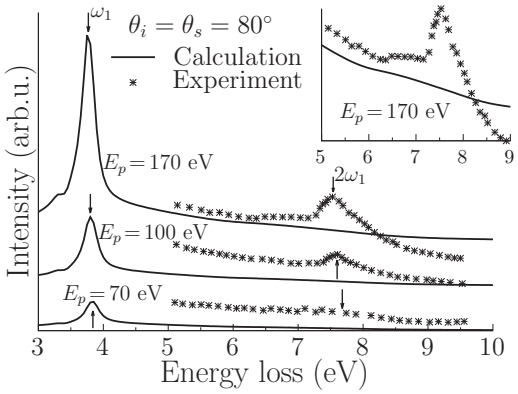

FIG. 7. Primary energy dependence of HREELS of Ag(111). Peaks on the experimental spectra are attributed to the double-plasmon excitation and are, accordingly, absent from the theoretical spectra. The inset shows the same spectra for $E_p = 170$ eV in a narrower energy range. The experimental data compiled from Ref. [17] are used.

Since our calculations based on Eq. (2) are linear with respect to the interaction between the probe electron and the electronic subsystem of the target (distorted wave [13] with the first Born approximation for inelastic processes), the multiple energy losses, e.g., multiple plasmon excitations, are beyond the capacity of this approach. Nonetheless, especially at higher primary energies, multiple losses can be expected in the experimental spectra. In Fig. 7 we plot the theoretical spectra together with the corresponding experimental ones for three different primary energies of 170, 100, and 70 eV at the specular geometry of $\theta_i = \theta_s = 80°$, where we now focus on the higher energy range. While the theoretical lines are rather smooth in this range, the experimental spectra at $E_p = 170$ and 100 eV have prominent peaks around 7.6 eV. Considering that (i) the positions of these peaks are very close to twice the energy of the strong single-plasmon peaks around 3.7 eV, (ii) their intensities change with E_p consistently with those of the corresponding single-plasmon peaks, and (iii) these peaks are present in the experiment but absent in the linear-response-based calculations, we are led to the conclusion that these peaks are due to the double-plasmon excitations.

To reproduce the multiple plasmons theoretically, a theory of EELS beyond the first Born approximation is required. We note that the formal theory of inelastic scattering of a quantum-mechanical particle to the *second* Born approximation, expressed in terms of the *quadratic* density-response function of a target, was constructed in Ref. [31]. The practical implementations of this theory have not, however, been yet developed.

IV. CONCLUSIONS

We have revisited the problem of energy losses by electrons in reflection electron energy-loss spectroscopy with the focus on the role of the probing electrons' kinematics. The inadequacy of the description of EELS in terms of the energy-loss functions has been emphasized for materials where the bulk and the surface features overlap or are close in energy in the

excitation spectra. We have implemented the theory including the effect of the detailed quantum-mechanical motion of the probe electrons during their energy losses, using the Ag surface as a representative example of a system where the kinematic aspect of the problem is particularly important.

Since our primary interest lies in the role of the kinematic effects, for the sophisticated problem of the d electrons' response, we have used a simplified model of the background dielectric function, which has immensely simplified the numerical implementation. As a side effect, although we have found reasonably good overall agreement with HREELS, at strongly off-specular geometries of the experiment, the theory and the measurements disagree. We have tracked this discrepancy down to the failure of the substitution of the d electrons with the background dielectric function to describe the dispersion of the main loss feature of 3.7 eV in Ag at larger values of the momentum. Thus the limits of the applicability of that otherwise very useful model have been set. This difficulty is anticipated to be overcome in the future theory, with all the ingredients included within the *ab initio* approach.

Another deviation of the theory from experiment we have found can be qualified as evidence of the consistency of the former rather than its deficiency. Namely, the experiment shows peaks at EEL spectra that, from all the evidence, can be attributed to the double-plasmon excitations. The linear-response theory, which our approach is based on, fundamentally cannot account for such losses, and we do not, accordingly, obtain the double-excitation peaks in the calculations. Future implementations of the theory of quadratic and higher-order response will be able to account for these processes.

ACKNOWLEDGMENTS

V.U.N. acknowledges support from the Ministry of Science and Technology, Taiwan, Grant No. 104-2112-M-001-007. This work was supported by the Spanish Ministry of Economy and Competitiveness MINECO (Project No. FIS2013-48286-C2-1-P).

APPENDIX: PROPERTIES OF THE MODEL OF THE BACKGROUND DF

In this Appendix we scrutinize the model of the background DF used in this paper to account for the d electrons in the dielectric response of silver [9,19]. For the sake of maximal clarity, we do this analytically by considering the bulk response. In this case the same model is determined by the DF

$$\varepsilon(q,\omega) = \varepsilon_{\mathrm{Ag}}(\omega) - \left[1 - \frac{\omega_p^2}{\omega^2}\right] + \varepsilon_{Ls}(q,\omega) = \varepsilon_d(\omega) + [\varepsilon_{Ls}(q,\omega) - 1], \quad \text{(A1)}$$

where $\varepsilon_{\mathrm{Ag}}(\omega)$ is the optical experimental DF of Ag, $\varepsilon_d(\omega)$ is given by Eq. (22), and $\varepsilon_{Ls}(q,\omega)$ is Lindhard's DF of the homogeneous electron gas [32], taken at the density of the s electrons of Ag.

In Fig. 8 we plot the energy-loss function using the DF of Eq. (A1) for several values of the wave vector q. The plasmon peak near 3.7 eV weakens with the increase of q until it disappears at $q \approx 0.2$ a.u. This is consistent with the behavior of the DF itself, which is plotted in Fig. 9. Indeed, for $q = 0$ and 0.1 a.u., Re $\varepsilon(q,\omega)$ crosses zero in the corresponding energy range, thereby producing the plasmon peak in the loss function. This is not the case any longer for $q = 0.15$, 0.175, and 0.2 a.u., although for the former two wave vectors, the peaks in question still persist in the loss function due to Re ε *approaching* the zero axis (see Ref. [11]). Last, at $q = 0.2$ a.u., Re ε is very far from zero in this ω range, and no peak in the loss function can be discerned any longer.

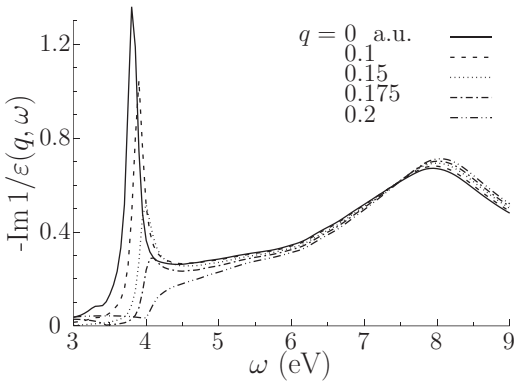

FIG. 8. The bulk energy-loss function using the DF of Eq. (A1) plotted for several values of the wave vector q. The plasmon peak near 3.7 eV clearly weakens and finally disappears with the increase of q.

The above results are consistent with those of Sec. III of this paper. Indeed, the main contribution to the z component of the wave vector of the external perturbation can be estimated from Eqs. (12), (6), and (9) as $p_z + p_z'$ (note that $p_z < 0$ and $p_z' > 0$). When $E_p = 40$ eV and $\theta_i = 80^\circ$, this is equal to 0.123 and 0.259 a.u. for $\theta_s = 75^\circ$ and 70°, respectively. The corresponding values of $q_\parallel$ are 0.117 and 0.160 a.u., respectively. Then $q = [(p_z + p_z')^2 + q_\parallel^2]^{1/2}$ are 0.170 and 0.304 a.u., respectively, explaining the presence of the plasmon near 3.7 eV in the theoretical spectra in the former and its

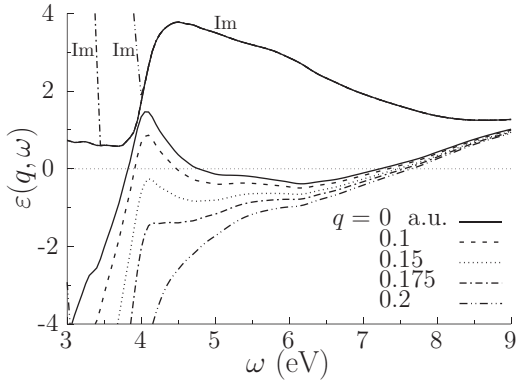

FIG. 9. The dielectric function of Eq. (A1). Lines without labels are the real parts of the DF at the corresponding values of q. Lines with the label "Im" are imaginary parts, which, for all values of q, largely coincide with $-\mathrm{Im}\,\varepsilon(q = 0,\omega)$ since the Lindhard's DF is real in the corresponding energy ranges.

absence in the latter case. For the specular geometry in Fig. 5, the corresponding value is $q = 0.09$ a.u., consistent with the strong theoretical lower-energy plasmon peak in this figure. The same argument holds for the spectra in Fig. 7.

Experimentally, however, this prediction of the model is not supported, as can be seen in Fig. 4 (top experimental spectrum): the plasmon near 3.7 eV persists in the measurements on Ag at larger wave vectors. We therefore can conclude that, at larger wave vectors, the response of d electrons cannot be realistically substituted with a wave-vector-independent dielectric function when it concerns the lower-energy plasmon in Ag, while this model is quite successful in the higher energy range, where the spectra are dominated by the response of s electrons outside the d-electron background [9,19].

[1] J. Hillier and R. F. Baker, Microanalysis by means of electrons, J. Appl. Phys. **15**, 663 (1944).

[2] H. Ibach and D. L. Mills, *Electron Energy Loss Spectroscopy and Surface Vibrations* (Academic, New York, 1982).

[3] T. Eberlein, U. Bangert, R. R. Nair, R. Jones, M. Gass, A. L. Bleloch, K. S. Novoselov, A. Geim, and P. R. Briddon, Plasmon spectroscopy of free-standing graphene films, Phys. Rev. B **77**, 233406 (2008).

[4] R. F. Egerton, Electron energy-loss spectroscopy in the TEM, Rep. Prog. Phys. **72**, 016502 (2009).

[5] D. Pines and P. Nozieres, *The Theory of Quantum Liquids* (Benjamin, New York, 1966).

[6] R. H. Ritchie, Plasma losses by fast electrons in thin films, Phys. Rev. **106**, 874 (1957).

[7] A. J. Bennett, Influence of the electron charge distribution on surface-plasmon dispersion, Phys. Rev. B **1**, 203 (1970).

[8] K.-D. Tsuei, E. W. Plummer, A. Liebsch, K. Kempa, and P. Bakshi, Multipole Plasmon Modes at a Metal Surface, Phys. Rev. Lett. **64**, 44 (1990).

[9] A. Liebsch, Prediction of a Ag multipole surface plasmon, Phys. Rev. B **57**, 3803 (1998).

[10] A. Liebsch, *Electronic Excitations at Metal Surfaces* (Plenum, New York, 1997).

[11] V. U. Nazarov, Electronic excitations in quasi-2D crystals: What theoretical quantities are relevant to experiment? New J. Phys. **17**, 073018 (2015).

[12] V. U. Nazarov, Analytical properties of dielectric response of semi-infinite systems and the surface electron energy loss function, Surf. Sci. **331-333**, 1157 (1995).

[13] J. R. Taylor, *Scattering Theory* (Wiley, New York, 1972).

[14] W. Kohn and L. J. Sham, Self-consistent equations including exchange and correlation effects, Phys. Rev. **140**, A1133 (1965).

[15] V. U. Nazarov, Multipole surface-plasmon-excitation enhancement in metals, Phys. Rev. B **59**, 9866 (1999).

[16] V. U. Nazarov and S. Nishigaki, Inelastic low energy electron diffraction at metal surfaces, Surf. Sci. **482-485**, 640 (2001).

[17] A. Politano, V. Formoso, and G. Chiarello, Collective electronic excitations in thin Ag films on Ni(111), Plasmonics **8**, 1683 (2013).

[18] Edited by Edward D. Palik, *Handbook of Optical Constants of Solids* (Academic, New York, 1985).

[19] A. Liebsch and W. L. Schaich, Influence of a polarizable medium on the nonlocal optical response of a metal surface, Phys. Rev. B **52**, 14219 (1995).

[20] In contrast to the Kohn-Sham χ_0, χ includes electron-electron interactions, and the two response functions are related as $\chi^{-1} = \chi_0^{-1} - 1/|\mathbf{r} - \mathbf{r}'| - f_{xc}$, where f_{xc} is the exchange-correlation kernel [24].

[21] In Refs. [12,16] the solution was given in the momentum space, of which Eq. (2) is the Fourier transform.

[22] P. J. Feibelman and D. E. Eastman, Photoemission spectroscopy—Correspondence between quantum theory and experimental phenomenology, Phys. Rev. B **10**, 4932 (1974).

[23] E. V. Chulkov, V. M. Silkin, and P. M. Echenique, Image potential states on metal surfaces: Binding energies and wave functions, Surf. Sci. **437**, 330 (1999).

[24] E. K. U. Gross and W. Kohn, Local Density-Functional Theory of Frequency-Dependent Linear Response, Phys. Rev. Lett. **55**, 2850 (1985).

[25] E. E. Krasovskii and W. Schattke, Surface electronic structure with the linear methods of band theory, Phys. Rev. B **56**, 12874 (1997).

[26] E. E. Krasovskii, W. Schattke, V. N. Strocov, and R. Claessen, Unoccupied band structure of $NbSe_2$ by very low-energy electron diffraction: Experiment and theory, Phys. Rev. B **66**, 235403 (2002).

[27] M. Rocca, Li Yibing, F. Buatier de Mongeot, and U. Valbusa, Surface plasmon dispersion and damping on Ag(111), Phys. Rev. B **52**, 14947 (1995).

[28] M. Rocca, Low-energy EELS investigation of surface electronic excitations on metals, Surf. Sci. Rep. **22**, 1 (1995).

[29] F. Moresco, M. Rocca, V. Zielasek, T. Hildebrandt, and M. Henzler, ELS-LEED study of electronic excitations on Ag(110) and Ag(111), Surf. Sci. **388**, 24 (1997).

[30] V. M. Silkin, P. Lazić, N. Došlić, H. Petek, and B. Gumhalter, Ultrafast electronic response of Ag(111) and Cu(111) surfaces: From early excitonic transients to saturated image potential, Phys. Rev. B **92**, 155405 (2015).

[31] V. U. Nazarov and S. Nishigaki, Z^3-order theory of quantum inelastic scattering of charges by solids, Phys. Rev. B **65**, 094303 (2002).

[32] J. Lindhard, On the properties of a gas of charged particles, Mat. Fys. Medd. K. Dan. Vidensk. Selsk. **28**, 1 (1954).